QUANTUM CRITICALITY

Singular charge fluctuations at a magnetic quantum critical point

L. Prochaska[1]*, X. Li[2]*†, D. C. MacFarland[1,3]*‡, A. M. Andrews[3], M. Bonta[4], E. F. Bianco[5]§, S. Yazdi[6]¶, W. Schrenk[7], H. Detz[7]#, A. Limbeck[4], Q. Si[8], E. Ringe[6]**, G. Strasser[3,7], J. Kono[2,6,8], S. Paschen[1,8]††

Strange metal behavior is ubiquitous in correlated materials, ranging from cuprate superconductors to bilayer graphene, and may arise from physics beyond the quantum fluctuations of a Landau order parameter. In quantum-critical heavy-fermion antiferromagnets, such physics may be realized as critical Kondo entanglement of spin and charge and probed with optical conductivity. We present terahertz time-domain transmission spectroscopy on molecular beam epitaxy–grown thin films of $YbRh_2Si_2$, a model strange-metal compound. We observed frequency over temperature scaling of the optical conductivity as a hallmark of beyond-Landau quantum criticality. Our discovery suggests that critical charge fluctuations play a central role in the strange metal behavior, elucidating one of the long-standing mysteries of correlated quantum matter.

Quantum critical behavior as prescribed by the Landau framework of order parameter fluctuations (*1*, *2*) has been clearly identified in insulating quantum magnets such as $LiHoF_4$ (*3*) and $TlCuCl_3$ (*4*). In strongly correlated metals, however, this framework often fails. In the strange-metal (*5*) regime of various correlated systems (*6*), electronic localization-delocalization transitions have been reported (*7*–*14*), and it is an outstanding question whether they are a key ingredient of beyond-Landau quantum criticality. To make progress, it is essential to study the dynamics of charge carriers in a suitable setting.

We chose the heavy fermion metal $YbRh_2Si_2$ (*15*) for our investigation because it has a well-defined quantum critical point (*15*, *16*) and shows evidence for an electron localization-delocalization transition (*7*, *8*) in its strange-metal regime. An ideal tool to study such properties is optical conductivity measurements in the relevant frequency window, which is typically the terahertz range and below for heavy fermion systems. However, such measurements are challenging on bulk samples because the Kramers-Kronig transformation to extract the real and imaginary parts of the optical conductivity from reflectivity measurements introduces substantial uncertainty at low frequencies (*17*). Thus, we resorted to a different approach: We performed terahertz time-domain transmission spectroscopy experiments on thin films of $YbRh_2Si_2$ grown by means of molecular beam epitaxy (MBE). Our measurements reveal ω/T scaling of the optical conductivity, where ω is the (angular) frequency and T is the temperature, elucidating the mechanism for strange-metal phenomena.

To grow epitaxial thin films of $YbRh_2Si_2$ on (terahertz transparent) Ge substrates (Fig. 1A), we used a specially equipped MBE system (*18*). The epitaxial growth of phase-pure $YbRh_2Si_2$ was confirmed with x-ray diffraction (Fig. 1B) (*18*), and the high quality of the film and the film-substrate interface were revealed with high-resolution transmission electron microscopy (Fig. 1, C and D) (*18*). The temperature dependence of the (quasi) dc electrical resistivity $\rho(T)$ of these films (*18*) is similar to that of bulk single crystals (Fig. 2) (*15*, *19*). $\rho(T)$ displays strange-metal behavior, $\rho = \rho_0 + A'T^{\alpha}$ (Fig. 2B), where A' is a constant, with an exponent α that strongly deviates from the Fermi liquid value $\alpha = 2$ and tends to $\alpha = 1$ in the low-temperature limit (fig. S1).

The frequency dependence of the real part of the complex optical conductivity, $\mathrm{Re}(\sigma)$, measured at temperatures between 1.4 and 250 K and frequencies between 0.25 and 2.6 THz, is shown in Fig. 3A [the imaginary part, $\mathrm{Im}(\sigma)$, is shown in fig. S2]. The dc electrical conductivity $\sigma = 1/\rho$ values, plotted as symbols at $\omega = 0$, are compatible with the extrapolation of the finite frequency results to zero frequency. Both $\mathrm{Re}(\sigma)$ and $\mathrm{Im}(\sigma)$ are flat and featureless at temperatures above ~80 K (indicating strong incoherent scattering of charges) but develop sizable temperature and frequency dependence at lower temperatures, with spectral weight of $\mathrm{Re}(\sigma)$ being transferred to low frequencies. The increasingly sharp and pronounced resonance of $\mathrm{Re}(\sigma)$, with non-Lorentzian shape (non-Drude behavior) (fig. S3), may in clean samples be associated with non–Fermi liquid behavior. These results confirm deviations from simple Drude behavior seen earlier in optical reflectivity measurements in the far-infrared range on bulk $YbRh_2Si_2$ single crystals (*20*).

To explore dynamical scaling, we analyzed the frequency-dependent intrinsic optical conductivity $\sigma_{\mathrm{in}}(\omega)$ by subtracting a residual resistivity because of impurity scattering; this subtraction is motivated by analogy to the Matthiessen's law used for the dc resistivity (*18*). We plot $\mathrm{Re}[\sigma_{\mathrm{in}}(\omega)] \cdot T^{\alpha}$ as a function of $\hbar\omega/(k_B T)$, where $\hbar$ is the Planck constant divided by 2π and k_B is the Boltzmann constant, for temperatures ($T \le 15$ K) well below the material's Kondo temperature $T_K = 24$ K (Fig. 3B) (*15*) and frequencies below 2 THz. For $\alpha \approx 1$, all curves collapse, demonstrating ω/T scaling of $\mathrm{Re}[\sigma_{\mathrm{in}}(\omega)]$.

How can the optical conductivity, which probes charge fluctuations, show critical ω/T scaling at an antiferromagnetic quantum critical point where a priori only spin fluctuations are expected—and indeed observed (*21*–*23*)—to be critical? A natural way for this to happen is to have a critical form of the Kondo entanglement between the local moments and the conduction electrons (*24*–*26*), as illustrated in Fig. 4. Across the quantum critical point, the conduction electrons go from being (asymptotically) decoupled from the local moments (Fig. 4, bottom left box) to being entangled with them (Fig. 4, bottom right box). Correspondingly, the elementary excitations change from separate charge (single conduction electrons or holes) and spin excitations (Fig. 4, top left box) to the heavy quasiparticles (Fig. 4, top right box) that are hybrids of the slow composite fermions (Fig. 4, large tadpole) and the bare conduction electrons (Fig. 4, small tadpole); the single-electron excitations capture the continuous onset of the Kondo entanglement at the quantum critical point and are part of the critical degrees of freedom. Thus, optical conductivity, which probes the charge current of the elementary excitations, manifests the singular fluctuations of the quantum critical point. Within the Landau description of a metallic antiferromagnetic quantum critical point (*1*, *2*),

[1]Institute of Solid State Physics, Technischen Universität (TU) Wien, Wiedner Hauptstraße 8-10, 1040 Vienna, Austria. [2]Department of Electrical and Computer Engineering, 6100 Main Street, Rice University, Houston, TX 77005, USA. [3]Institute of Solid State Electronics, TU Wien, Nanocenter Campus Gußhaus, Gußhausstraße 25-25a, Gebäude CH, 1040 Vienna, Austria. [4]Institute of Chemical Technologies and Analytics, TU Wien, Getreidemarkt 9, 1060 Vienna, Austria. [5]Department of Chemistry, 6100 Main Street, Rice University, Houston, TX 77005, USA. [6]Department of Materials Science and Nanoengineering, 6100 Main Street, Rice University, Houston, TX 77005, USA. [7]Center for Micro- and Nanostructures, TU Wien, Nanocenter Campus Gußhaus, Gußhausstraße 25-25a, Gebäude CH, 1040 Vienna, Austria. [8]Department of Physics and Astronomy, Center for Quantum Materials, 6100 Main Street, Rice University, Houston, TX 77005, USA.
*These authors contributed equally to this work. †Present address: Department of Physics, California Institute of Technology, Pasadena, CA 91125, USA; and Institute for Quantum Information and Matter, California Institute of Technology, Pasadena, CA 91125, USA. ‡Present address: State University of New York–University at Buffalo, Jacobs School of Medicine and Biomedical Sciences, 955 Main Street, Buffalo, NY 14203, USA. §Present address: Kavli Institute at Cornell for Nanoscale Science, Cornell University, Ithaca, NY 14853, USA. ¶Present address: Renewable and Sustainable Energy Institute, University of Colorado Boulder, Boulder, CO 80309, USA. #Present address: Central European Institute of Technology, Brno University of Technology, Purkyňova 123, Brno, 612 00, Czech Republic. **Present address: Department of Earth Sciences, University of Cambridge, Downing Street, Cambridge CB2 3EQ, UK; and Department of Materials Science and Metallurgy, University of Cambridge, 27 Charles Babbage Road, Cambridge CB3 0FS, UK.
††Corresponding author. Email: paschen@ifp.tuwien.ac.at

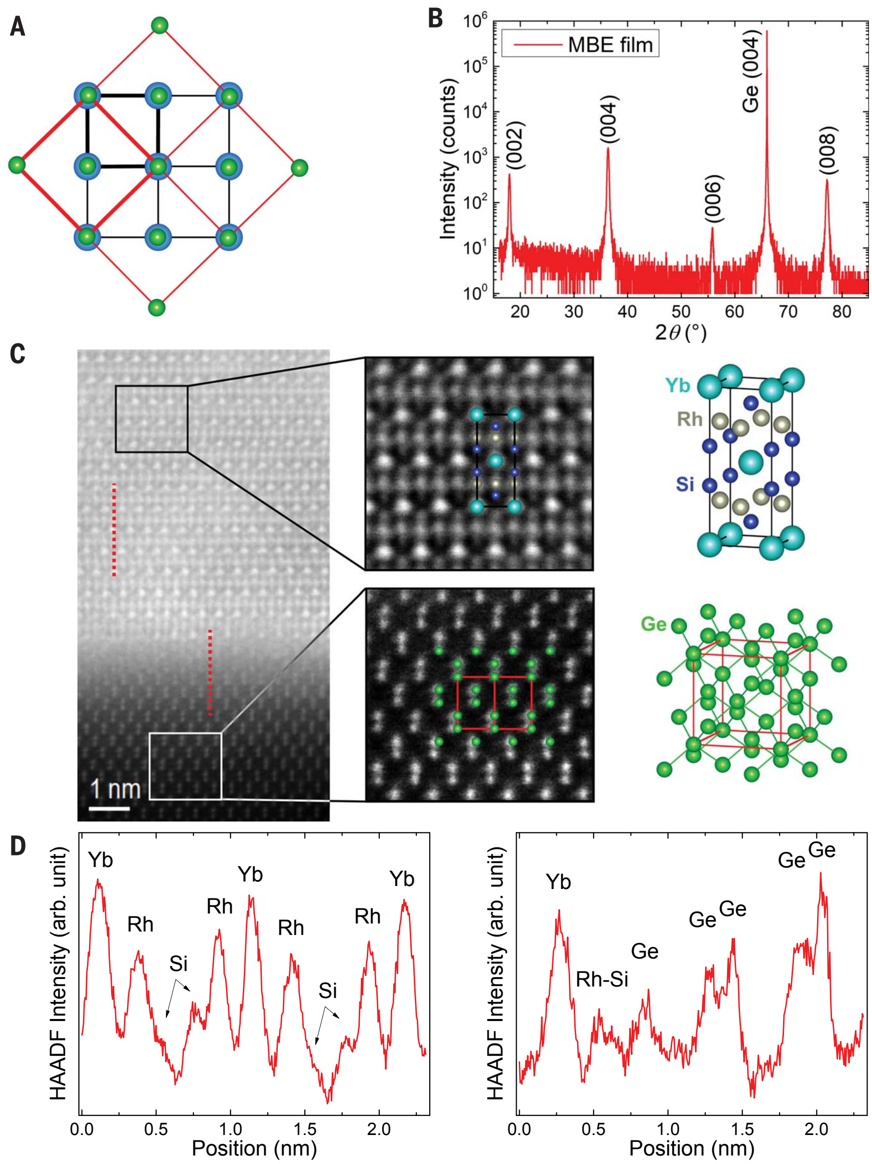

Fig. 1. $YbRh_2Si_2$ thin films grown by means of MBE. (**A**) Visualization of the lattice matching between $YbRh_2Si_2$ (blue circles and black lines) and Ge (green circles and red lines), with the crystallographic *c* directions pointing out of the plane. For the Yb atoms to associate with the Ge atoms, the respective unit cells (thick lines) [(C), right] are rotated by 45° with respect to each other around the *c* direction. (**B**) High-resolution x-ray diffraction pattern, with all peaks identified as due to the (about 40 nm thick) film or the Ge substrate, confirming that the film is phase-pure $YbRh_2Si_2$. (**C**) Atomic-resolution high-angle annular dark field scanning transmission electron microscopy (HAADF-STEM) image of the interface between film (top left) and substrate (bottom left), representative enlarged views with simulated overlays (center), and the corresponding unit cells (right). (**D**) Intensity profiles along the red dotted lines in (C). The left and right panels correspond to the top red dotted line within the film and the bottom red dotted line across the interface, respectively.

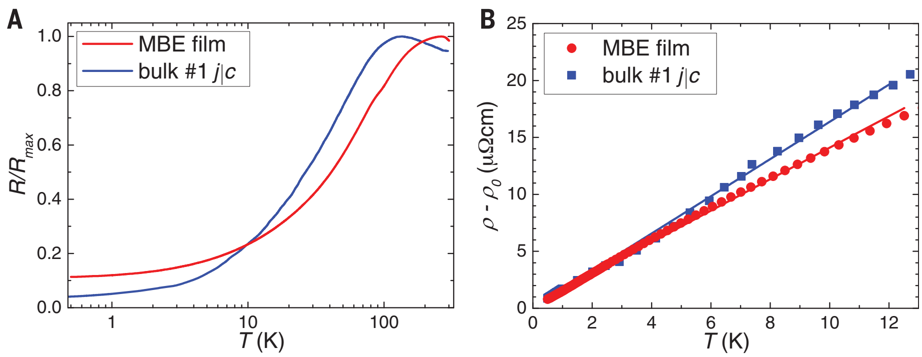

Fig. 2. Electrical resistivity of MBE-grown $YbRh_2Si_2$. (**A**) Normalized resistance of an MBE-grown $YbRh_2Si_2$ film and a bulk single crystal with current *j* within the tetragonal *aa* plane (*15*) for comparison. The film was measured by using the van der Pauw technique. (**B**) Corresponding low-temperature resistivities, with the residual resistivities [ρ_0 = 11.6 and 2.45 microhm cm for the MBE and bulk (*15*) samples, respectively, determined by linear-in-*T* fits to the data below 1 K] subtracted, displaying non–Fermi liquid behavior (lines represent $\rho - \rho_0 = A'T^\alpha$ fits with a constant exponent α to the data below 12 K; the temperature dependence of α is provided in fig. S1).

the slow long-wavelength fluctuations of the order parameter alone describe a Gaussian fixed point, where ω/T scaling is violated. The incorporation of the single-electron excitations in the quantum critical spectrum not only makes charge fluctuations part of the quantum criticality but also turns the fixed point into an interacting one (*24*), leading to ω/T scaling.

Dynamical scaling of the optical conductivity in the region of *T*-linear resistivity has also been analyzed in an optimally doped Bi-2212 cuprate (*27*). There, different scaling functions are needed in different ω/T ranges, leaving open the question of how the fluctuations of the charge carriers connect with the robust linear-in-temperature resistivity of the cuprate superconductors. By contrast, in the present study of $YbRh_2Si_2$, a single ω/T scaling form

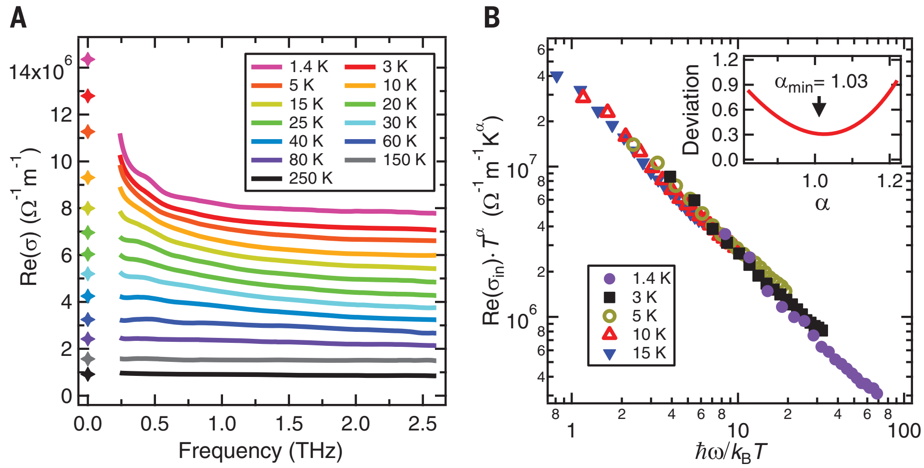

Fig. 3. Terahertz time-domain transmission spectroscopy of MBE-grown $YbRh_2Si_2$. (**A**) Real part of optical conductivity Re(σ) versus frequency at different temperatures (bottom to top: 250, 150, 80, 60, 40, 30, 25, 20, 15, 10, 5, 3, and 1.4 K), with corresponding dc values marked as zero-frequency points. Curves below 250 K (and the respective dc values) are successively offset by 6×10^5 ohm^{-1} m^{-1} for clarity. (**B**) ω/T scaling, with a critical exponent of $\alpha \approx 1$, revealed with $\mathrm{Re}[\sigma_{in}(\omega)] \cdot T^{\alpha}$ isotherms plotted versus $\hbar\omega/(k_B T)$ collapsing onto a single curve for temperatures $T \leq 15$ K and frequencies below 2 THz. (Inset) Normalized deviation between the different isotherms as a function of α, revealing best scaling for α = 1.03.

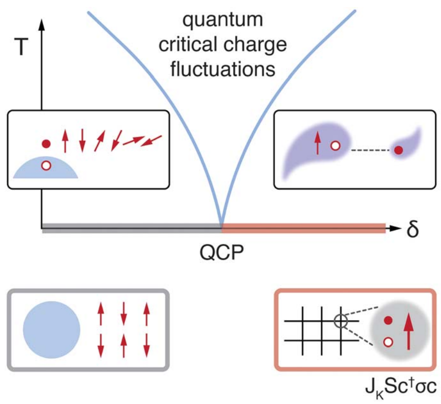

Fig. 4. Illustration of quantum-critical charge fluctuations emerging from Kondo disentanglement. Tuning a heavy fermion metal with a nonthermal parameter δ, which microscopically corresponds to the ratio of Kondo to RKKY coupling, from an antiferromagnetic ground state with local moment order (bottom left box; blue circle and red arrows indicate Fermi sphere and local moments, respectively) to a Kondo entangled paramagnet (bottom right box; the antiferromagnetic Kondo exchange J_K favors the formation of a Kondo singlet between the local moment S, represented as an arrow, and the spin of the conduction electrons $c^{\dagger}\sigma c$—the particle-hole excitation of the Fermi sea in the spin-triplet channel) creates distinct single-particle excitations (top boxes) and, in turn, quantum-critical charge fluctuations within the quantum-critical fan.

is uncovered in its strange metal regime. It is important to explore the dynamical scaling of the optical conductivity in other materials classes with strange-metal behavior; one can then assess whether the charge carrier dynamics emerging from a localization-delocalization quantum critical point, as proposed here, is a universal mechanism of strange-metal behavior. This scaling form also provides an intriguing link to the quantum scaling of metal-insulator transitions, both in Mott-Hubbard (*28–30*) and in disordered systems (*31*).

Our results demonstrate that charge carriers are a central ingredient of the singular physics at the border of antiferromagnetic order, providing direct evidence for the beyond-Landau nature of metallic quantum criticality. Our findings also delineate the role of electronic localization transitions in strange-metal phenomena, which are relevant to a variety of strongly correlated materials (*32*) and beyond (*33*).

REFERENCES AND NOTES

1. J. A. Hertz, *Phys. Rev. B Condens. Matter* **14**, 1165–1184 (1976).
2. A. J. Millis, *Phys. Rev. B Condens. Matter* **48**, 7183–7196 (1993).
3. D. Bitko, T. F. Rosenbaum, G. Aeppli, *Phys. Rev. Lett.* **77**, 940–943 (1996).
4. P. Merchant *et al*., *Nat. Phys.* **10**, 373–379 (2014).
5. P. Giraldo-Gallo *et al*., *Science* **361**, 479–481 (2018).
6. J. A. N. Bruin, H. Sakai, R. S. Perry, A. P. Mackenzie, *Science* **339**, 804–807 (2013).
7. S. Paschen *et al*., *Nature* **432**, 881–885 (2004).
8. S. Friedemann *et al*., *Proc. Natl. Acad. Sci. U.S.A.* **107**, 14547–14551 (2010).
9. J. Custers *et al*., *Nat. Mater.* **11**, 189–194 (2012).
10. Y. Luo *et al*., *Nat. Mater.* **13**, 777–781 (2014).
11. F. F. Balakirev *et al*., *Nature* **424**, 912–915 (2003).
12. H. Oike, K. Miyagawa, H. Taniguchi, K. Kanoda, *Phys. Rev. Lett.* **114**, 067002 (2015).
13. S. Badoux *et al*., *Nature* **531**, 210–214 (2016).
14. Y. Cao *et al*., *Nature* **556**, 43–50 (2018).
15. O. Trovarelli *et al*., *Phys. Rev. Lett.* **85**, 626–629 (2000).
16. P. Gegenwart *et al*., *Phys. Rev. Lett.* **89**, 056402 (2002).
17. J. Orenstein *et al*., *Phys. Rev. B Condens. Matter* **42**, 6342–6362 (1990).
18. Materials and methods are available as supplementary materials.
19. T. Westerkamp, thesis, TU Dresden, Germany (2009).
20. S. Kimura *et al*., *Phys. Rev. B Condens. Matter* **74**, 132408 (2006).
21. M. C. Aronson *et al*., *Phys. Rev. Lett.* **75**, 725–728 (1995).
22. A. Schröder *et al*., *Nature* **407**, 351–355 (2000).
23. C. Stock *et al*., *Phys. Rev. Lett.* **109**, 127201 (2012).
24. Q. Si, S. Rabello, K. Ingersent, J. L. Smith, *Nature* **413**, 804–808 (2001).
25. P. Coleman, C. Pépin, Q. Si, R. Ramazashvili, *J. Phys. Condens. Matter* **13**, R723–R738 (2001).
26. T. Senthil, M. Vojta, S. Sachdev, *Phys. Rev. B Condens. Matter Mater. Phys.* **69**, 035111 (2004).
27. D. van der Marel *et al*., *Nature* **425**, 271–274 (2003).
28. T. Senthil, *Phys. Rev. B Condens. Matter* **78**, 035103 (2008).
29. H. Terletska, J. Vučičević, D. Tanasković, V. Dobrosavljević, *Phys. Rev. Lett.* **107**, 026401 (2011).
30. T. Furukawa, K. Miyagawa, H. Taniguchi, R. Kato, K. Kanoda, *Nat. Phys.* **11**, 221–224 (2015).
31. H. Lee, J. P. Carini, D. V. Baxter, W. Henderson, G. Grüner, *Science* **287**, 633–636 (2000).
32. B. Keimer, J. E. Moore, *Nat. Phys.* **13**, 1045–1055 (2017).
33. P. T. Brown *et al*., *Science* **363**, 379–382 (2019).
34. L. Prochaska, X. Li, D. C. MacFarland, A. M. Andrews, M. Bonta, E. F. Bianco, S. Yazdi, W. Schrenk, H. Detz, A. Limbeck, Q. Si, E. Ringe, G. Strasser, J. Kono, S. Paschen, Data for the publication "Singular charge fluctuations at a magnetic quantum critical point." Zenodo (2019); doi:10.5281/zenodo.3541572.

ACKNOWLEDGMENTS

We thank P. Gegenwart, Y.-B. Kim, H. von Löhneysen, S. Nakatsuji, H.-C. Nägerl, and A. Prokofiev for useful discussions. **Funding:** Financial support for this work was provided by the European Research Council (ERC Advanced Grant 227378), the U.S. Army Research Office (ARO W911NF-14-1-0496), the Austrian Science Fund (FWF W1243, P29279-N27, and P29296-N27), and the European Union's Horizon 2020 research and innovation program (grant agreement 824109-EMP). X.L. and J.K. acknowledge financial support from the National Science Foundation (NSF MRSEC DMR-1720595) and the ARO (W911NF-17-1-0259). Q.S. acknowledges financial support from the NSF (DMR-1920740), the Robert A. Welch Foundation (C-1411), and the ARO (W911NF-14-1-0525) and the hospitality of the University of California at Berkeley, the Aspen Center for Physics (NSF grant PHY-1607611), and the Los Alamos National Laboratory (through a Ulam Scholarship from the Center for Nonlinear Studies). This work has also been supported by an InterDisciplinary Excellence Award (IDEA) from Rice University (Q.S., E.R., J.K., and S.P.). **Author contributions:** S.P. designed and led the research. L.P., D.C.M., A.M.A., W.S., H.D., and G.S. performed the MBE growth. M.B. and A.L. performed the analytical characterization. E.F.B., S.Y., and E.R. performed the TEM investigation. X.L. and J.K. performed the terahertz spectroscopy. Q.S. contributed to the understanding of the results. L.P., X.L., D.C.M., Q.S., and S.P. wrote the manuscript, with contributions from all other authors. **Competing interests:** The authors have no competing interests. **Data and materials availability:** All data presented in this paper are deposited in Zenodo (*34*).

SUPPLEMENTARY MATERIALS

science.sciencemag.org/content/367/6475/285/suppl/DC1
Materials and Methods
Figs. S1 to S6
References (*35–53*)

6 August 2018; resubmitted 7 September 2019
Accepted 5 December 2019
10.1126/science.aag1595

Science

Singular charge fluctuations at a magnetic quantum critical point

L. Prochaska, X. Li, D. C. MacFarland, A. M. Andrews, M. Bonta, E. F. Bianco, S. Yazdi, W. Schrenk, H. Detz, A. Limbeck, Q. Si, E. Ringe, G. Strasser, J. Kono and S. Paschen

Science **367** (6475), 285-288.
DOI: 10.1126/science.aag1595

Spin-charge entanglement

Many physical properties follow characteristic scaling laws near quantum critical points, which are associated with phase transitions at absolute zero temperature. The material $YbRh_2Si_2$ has an antiferromagnetic quantum critical point, where spin-related properties are expected to follow such a scaling. Unexpectedly, Prochaska *et al.* found that charge fluctuations follow a critical scaling as well. The researchers fabricated high-quality thin films of $YbRh_2Si_2$ and used transmission spectroscopy to measure the optical conductivity of the film and infer the scaling. Their findings point to a highly entangled state of charge and spin, which may also be responsible for the strangemetal phase in this material.

Science, this issue p. 285

Science (print ISSN 0036-8075; online ISSN 1095-9203) is published by the American Association for the Advancement of Science, 1200 New York Avenue NW, Washington, DC 20005. The title *Science* is a registered trademark of AAAS.